OPTI 2014
An International Conference on
Engineering and Applied Sciences Optimization
M. Papadrakakis, M.G. Karlaftis, N.D. Lagaros (eds.)
Kos Island, Greece, 4-6, June 2014

ON SOME SHAPE AND TOPOLOGY OPTIMIZATION PROBLEMS IN CONDUCTIVE AND CONVECTIVE HEAT TRANSFERS

Gilles MARCK[1], **Yannick PRIVAT**[1]

[1]Laboratoire Jacques-Louis Lions
Pierre and Marie Curie University (Paris VI)
4, place Jussieu, 75252 Paris, FRANCE
e-mail: {gilles.marck,yannick.privat}@ljll.math.upmc.fr

Keywords: topology optimization, heat transfer, conduction, convection, laminar flow.

Abstract. *The topology optimization of systems subject to heat and mass transfers shows a wide potential for designing optimal and innovative structures in energy engineering. The present works apply the concepts of the homogenization method to two configurations subject to conductive and convective heat transfers. After recalling some basic principles, a special attention is given to the numerical approach dealing with multi-objective optimization problems that naturally occurs in several practical case studies. The two last sections are dedicated to some numerical investigations and provide a physical interpretation of the structural features reached by the optimization process. The main conclusion deals with the possibility of finding an acceptable trade-off between different objective functions, for both conductive and convective shape optimization problems, provided that the Pareto frontier is convex.*

1 INTRODUCTION

Heat and mass transfers are two physical phenomena at the root of several thermal systems. Shape and topology optimization problems in connection with this field are investigated through this proceeding, mainly from a numerical point of view, and a special attention is given to two heat transfer modes, respectively conduction and convection. They are both addressed by means of the same numerical approach, the so-called homogenization method [1], also referred as the Solid Isotropic Material with Penalization method (SIMP) [2]. Succinctly, the different shape optimization problems are transformed into topological ones by conveniently adapting the coefficients of the Partial Differential Equations (PDE) involved in their physical modelling. This allows solving only one set of equations even if the problems deal with subdomains characterized by different physical properties.

An overview of the main principles, such as the algorithm and some mathematical background, is provided in first section. The strategy used to properly handle the multi-objective nature of heat transfer problems is also detailed. Indeed, from a engineering point of view, most of industrial problems may be tackled by optimizing several objective functions at the same time, leading to a set of optimal solutions, the so-called Pareto set. However, establishing these optimal sets is computationally expensive and requires a suitable method to accurately capture the trade-offs between each solution.

The second and third sections are dedicated to the physical analysis of several numerical results. First, we consider a topology optimization problem in conduction: it aims at determining the best shape of a high conductivity layer located above a solid-state finite-size volume generating heat. This academic case has been introduced by Bejan [3] and has been studied with several different methods, ranging from physical approaches to genetic algorithms[4, 5, 6]. It has also been investigated in several articles using methods coming from the topology or shape optimization theory [7, 8, 9, 10], but without dealing with the multi-objective nature of the problem.

Secondly, we consider a similar topology optimization problem, but by expanding the physical modelling to take into account the influence of fluid motions on heat transfer. Consequently, the problem becomes more complex, since it attempts to establish the distribution of solid and fluid subdomains optimizing several objective functions subject to the Navier-Stokes and energy equations. On the one hand, a classical objective aims at minimizing the viscous dissipation occurring through the fluid phase, in order to minimize the power required to set it into motion. On the other hand, an objective relying on the thermal aspects of the problem pursue to maximize the heat transfer taking place inside the solid domain.

Minimizing the viscous dissipation of a fluid flow thanks to a topology optimization approach has initially been investigated by Borrvall and Petersson, in the frame of Stokes flow [11]. This first work has been followed by several studies using the same optimization strategy but with different physical models, such as Navier-Stokes [12], Darcy-Stokes [13] or unsteady Navier-Stokes [14]. More recently, several studies have studied the coupling of Navier-Stokes with a transport equation, such as the energy equation, in order to increase the performances of thermal systems [15, 16, 17]. However, only [18, 19] looks at establishing the set of optimal solutions underlining the trade-off taking place in the design of each structure.

2 ALGORITHM AND BASIC PRINCIPLES

2.1 Topology optimization problem

Fig. 1 pictures two common problems that occur in the enhancements of heat transfer systems. These both cases are considered under steady-state regime for this whole proceeding. On the left-hand side, the layout of two solid-state sub-domains, called Ω_0 and Ω_1, is optimized for a given functional. Both solid subdomains are characterized by two different thermal conductivities, respectively k_0 and k_1, and two different heat generation rate, respectively q_0 and q_1. Since no transport mechanism takes place inside the whole optimization domain, denoted $\Omega = \Omega_0 \cup \Omega_1$, the stationary heat equation for conduction may accurately describe the temperature behaviour.

By extension, the right-hand side of Fig. 1 illustrates a configuration where a convection phenomenon occurs in presence of a fluid flow. In this arrangement, one of the previous solid-state subdomain, for instance Ω_0, is replaced by a fluid phase flowing through the subdomain denoted Ω_f. On the other hand, the complementary subdomain remains in a solid state and is called Ω_s. Therefore, it means that the heat flux is conducted trough Ω_s, then convected by the flow motion inside Ω_f, leading to consider a conducto-convection phenomenon over the whole domain $\Omega = \Omega_f \cup \Omega_s$.

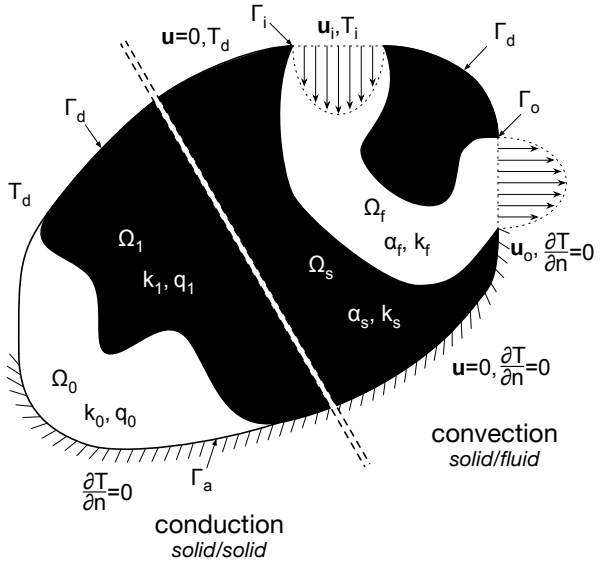

Figure 1: Conductive (left-hand side) and convective (right-hand side) shape and topology optimization problem in the frame of heat transfers.

For both problems, the thermal boundary conditions applied along $\partial\Omega$, also denoted Γ for the sake of clarity, are the following:

- the Dirichlet boundary condition, setting a constant temperature along the edge Γ_d;
- the Neumann boundary condition, setting a zero normal flux along the edge Γ_a. It is also referred as the adiabatic boundary condition in thermal engineering. By definition, it means that $\nabla T \cdot n \equiv \partial T/\partial n = 0$ where n is the normal vector to the boundary Γ pointing outwards the domain Ω.

In addition, the fluid flow boundary conditions are of two kinds:

- the walls, such as Γ_a or Γ_d are subject to a non-slip boundary conditions, assuming that $\mathbf{u} = 0$;
- the inlet and outlet flows are set up with a parabolic Poiseuille profile, fulfilling the law of conservation over the whole domain Ω.

Without giving details of the physical modelling leading to the different sets of PDE (see [10, 19] for further explanations), the different topology optimization problems may be generically written as

$$\begin{array}{ll} \inf\limits_{\chi_\omega \in \mathcal{D}_{\overline{\varphi}}} & J(\chi_\omega) = \displaystyle\int_\Omega f(\zeta, \chi_\omega, x) dx \\ \text{subject to} & \text{PDE with respect to variables } \zeta. \end{array} \tag{1}$$

and where $\mathcal{D}_{\overline{\varphi}} = \{\chi_\omega \in L^\infty(\Omega, \{0,1\}),\ |\omega| \leq \overline{\varphi}|\Omega|\}$. In this definition, ω is the subdomain whose is subject to the topology optimization process, that is Ω_1 or Ω_f, and χ_ω is its characteristic function. In addition, the feasible region $\mathcal{D}_{\overline{\varphi}}$ is restricted by a volume constraint on $|\omega|$, expressed as a fraction $\overline{\varphi} \in [0,1]$ of the whole volume domain $|\Omega|$. Indeed, for most optimization problems, $\omega = \Omega$ is the best trivial solution for several classes of objective functions $J(\chi_\omega)$, but is either unrealistic from an engineering point view or too expensive due to economic aspects.

2.2 Algorithm for homogenization method

As pointed out in the introduction, the topology optimization approach aims at conveniently adapting the coefficients of PDE to solve only one set of equations over the whole domain Ω. For instance, in the case of the conduction optimization problem, the thermal conductivity over Ω is given by

$$k(\chi_{\Omega_1}) = k_0 + (k_1 - k_0)\chi_{\Omega_1}. \tag{2}$$

This allows solving only one equation without explicitly taking into account the differences between the subdomains Ω_0 and Ω_1, apart from the thermal conductivity computation step. This idea is also applied to the heat generation rate q or Navier-Stokes equation, as detailed in the sections 3 and 4.

It is well known that the solutions of such infinite dimensional parametric problem do not necessarily exist (see [20, 21]), especially in the frame of heat conduction. To overcome this difficulty, a relaxation procedure is carried out: it mainly aims at extending the admissible set of solutions by replacing $\chi_\omega \in L^\infty(\Omega, \{0,1\})$ by $\eta \in L^\infty(\Omega, [0,1])$. From now on, any physical scalar parameter depending on χ_ω continuously depends on the function η. This feature can be exploited to cleverly control the convergence process by adding a penalization parameter p (see [2]). For example, the same thermal conductivity k now writes

$$k(\eta) = k_0 + (k_1 - k_0)\eta^p \quad \text{with} \quad 0 \leq \eta \leq 1 \quad \text{and} \quad p \geq 1. \tag{3}$$

The penalization parameter p masters the convexity of function $k(\eta)$ and allows tuning the convergence of the optimization problem. Other functions may be considered, while the penalization parameter p impacts on their convexity (see [19] for further details). Combined with other numerical tools such as filtering, it allows speeding up or slowing down the convergence and escaping from some local optima. Note that from this point, since the design parameters η are continuous, the domain Ω includes "composite" materials, with physical values ranging between their bounds defined in each subdomains Ω_0 and Ω_1. Consequently, one main role of the

penalization parameter is to ensure that the optimization process converges toward a *black and white* design: it progressively suppresses the *gray* level by penalizing the objective function.

Behind the non-existence issue, the second advantage of the relaxation step is to allow computing the topology derivative from the parametric formulation. Let denote $\langle dJ(\eta), \theta \rangle$, the differential of J with respect to η in direction θ. This topology derivative, also referred as sensitivity, is computed thanks to an adjoint state, which may be formulated from either the continuous or discrete forms of the EDP used as a constraint in problem (1). Such computations are expensive either from a mathematical or programming point of view: the corresponding numerical strategies are detailed in [10, 19]and are beyond the scope of this proceeding for the purpose of brevity.

The main sequence optimizing the objective function $J(\eta)$ is detailed in Alg. 1 [2]. The computation of the objective function is not detailed here: the instruction $J \leftarrow J(\eta, \mathbf{p})$ means that a finite volume solver computes the solution of the corresponding EDP in order to evaluate the objective functions. Note that the penalization parameter is a vector from now on: indeed, different penalizations may be used in agreement with the physical modelling.

The algorithm itself is based on an inner loop, which is nested within an outer loop. The inner loop aims at solving the optimization problem for a given state of the penalization parameters, whereas the outer loop controls them and is responsible for the convergence test leading to exit the whole algorithm.

$J_i \leftarrow \Theta$;
$J \leftarrow \mathrm{J}(\eta, \boldsymbol{p}_0)$;
for $j \leftarrow 0$ **to** ℓ **do**
  while $|J - J_i| \geq \epsilon_{i,j}$ **do**
    $J_i \leftarrow J$;
    compute $\langle dJ(\eta), \theta \rangle$;
    compute $\langle \widetilde{dJ}(\eta_h), \theta \rangle$ with r_j ;
    compute $\varphi(\eta)$ and $\langle d\varphi(\eta), \theta \rangle$;
    create MMA subproblem ;
    while $r_{IP} \geq \epsilon_{IP}$ **do**
      interior-point method iteration ;
    end
    $J \leftarrow \mathrm{J}(\eta, \boldsymbol{p}_j)$;
  end
end

Algorithm 1: Main algorithm for the homogenization method with an inner loop (indexed with i) nested inside an outer loop (indexed with j).

The inner loop sequentially computes the shape derivative $\langle dJ(\eta), \theta \rangle$, its numerically filtered form $\langle \widetilde{dJ}(\eta_h), \theta \rangle$, as well as the problem constraints and their gradient, respectively denoted $\varphi(\eta)$ and $\langle d\varphi(\eta), \theta \rangle$. These variables becomes the inputs of the Method of Moving Asymptotes (MMA), which belongs to a comprehensive class of gradient optimization methods based on conservative convex approximations. MMA has been shown to be particularly efficient for solving inequality-constrained non-linear programming problems, especially in the frame of structural and parametric optimization [22, 23]. Once a new state η have been generated, the set of EDP is solved again and the algorithm loops until the convergence criterion $\epsilon_{i,j}$ is satisfied.

The outer loop is indexed by means of an integer j ranging from 0 to a fixed number of iterations ℓ. This index drives three inner different parameters: the residual $\epsilon_{i,j}$, the penalization parameter $\mathbf{p}_j$, and the radius r_j of the filter applied to the shape derivative. This numerical filter is a convolution product involving the field of discrete design parameter η_i and writes [2],

$$\langle \widetilde{dJ}(\eta_i), \theta \rangle = \frac{\sum_{\ell=1}^{N} \eta_\ell \, H_\ell \, \langle dJ(\eta_\ell), \theta \rangle}{\eta_i \sum_{\ell=1}^{N} H_\ell} \tag{4}$$

where N is the number of discrete elements satisfying $|\mathbf{x}_i - \mathbf{x}_\ell| \leq r$ and $H_\ell = r - |\mathbf{x}_i - \mathbf{x}_\ell|$. This step aims at avoiding the so-called *checkerboard* problems leading to unrealistic optimal configurations due to the discretization process.

2.3 Strategy for bi-objective optimization

For many real optimization problems, the challenge is to conjointly optimize at least two or more objective functions in order to reach a configuration being a trade-off between these several objectives. A trade-off means that further optimization of one objective function decreases the performances of the other ones. This strategy leads to multiple solutions, referred to as the Pareto front. For instance, if the optimization problem is bi-objective, it can be written as

$$\inf_{\chi \in \mathcal{D}_{\overline{\varphi}}} J_1, \ \inf_{\chi \in \mathcal{D}_{\overline{\varphi}}} J_2 \tag{5}$$

subject to the EDP of problem (1). A suitable strategy allowing reaching the Pareto front lies on a linear combination of both objectives, which is also known as the aggregated objective function method. This approach can only generates the convex part of the Pareto frontier: consequently, this feature is assumed during the computational phase and will be checked afterwards. However, before linearly combining the different objective functions, they must be rescaled in order that the solutions reach an homogenous distribution along the Pareto frontier. This rescaling writes

$$\hat{J} = \frac{J - \underline{J}}{\overline{J} - \underline{J}} \tag{6}$$

where $\underline{J}$ and $\overline{J}$ respectively stands for the inferior and superior bounds of J functions. Consequently, before computing an optimal design for an aggregated objective function made of n objectives, it is required to solve $2n$ optimization problems. Then, for example if $n = 2$, the Pareto front may be outlined by minimizing J with several different values of $w \in [0, 1]$, where J writes

$$J(\eta) = w\hat{J}_1(\eta) + (1 - w)\hat{J}_2(\eta). \tag{7}$$

3 OPTIMAL SHAPE FOR CONDUCTIVE HEAT TRANSFER

Recalling the notation of Fig. 1, the non-relaxed topology optimization problem in conduction writes

$$\begin{aligned} \inf_{\chi_{\Omega_1} \in \mathcal{D}_{\overline{\varphi}}} \quad & J(\chi_{\Omega_1}) \\ \text{subject to} \quad & -\nabla \cdot (k(\chi_{\Omega_1}) \nabla T) = q(\chi_{\Omega_1}) \end{aligned} \tag{8}$$

where $\mathcal{D}_{\overline{\varphi}} = \{\chi_{\Omega_1} \in L^\infty(\Omega, \{0, 1\}), \ |\Omega_1| \leq \overline{\varphi}|\Omega|\}$ and two objective functions $J(\chi_{\Omega_1})$ are defined below. The heat equation should be completed with the boundary conditions introduced

in section 1. This problem aims at finding the optimal shape of a high-conductivity layer made of expensive raw material, such as copper for instance. Without the volume constraint $\overline{\varphi}$, the best trivial solution for most of objective functions is to cover the whole domain Ω with such material.

3.1 Objective functions

This problem has been mainly studied to address the efficient cooling of small electronic devices. Such components require high-conductivity networks cleverly allocated over their printed circuit board, since the more they are miniaturized, the more their heat generation rate increases. One obvious objective function deals with the minimization of the mean temperature over the domain Ω, in order to prevent damaging the electronic components due to overheating phenomena. This objective function simply writes

$$J_1(\chi_{\Omega_1}) = \frac{1}{|\Omega|}\int_\Omega T d\Omega. \tag{9}$$

A less straightforward goal aims at ensuring that the temperature field over the components remains as homogeneous as possible. This requirement comes from the necessity of the electronic device to communicate with its different sections. Since the computational frequency is directly linked with the silicon temperature, it is required to keep it as constant as possible in order to avoid any overload within the communication process. Consequently the second objective functional corresponds to the minimization of the temperature variance over the whole domain Ω and writes

$$J_2(\chi_{\Omega_1}) = \frac{1}{|\Omega|}\int_\Omega \left(T - J_1(\chi_{\Omega_1})\right)^2 dx = \frac{1}{|\Omega|}\int_\Omega T^2 dx - J_1^2(\chi_{\Omega_1}). \tag{10}$$

Even though both expressions are strictly equivalent, the last one is more efficient to work with, especially for computing the adjoint expression and the topology derivative $\langle dJ_2(\chi_\Omega), \theta\rangle$.

3.2 Numerical results

The numerical case investigated is well-known as the volume-to-point heat conduction problem [3]. It has been initially disclosed in 1997 and has been defined as:

> Consider a finite-size volume in which heat is being generated at every point, and which is cooled through a small patch (heat sink) located on its boundary. A finite amount of high conductivity (k_p) material is available. Determine the optimal distribution of k_p material through the given volume such that the highest temperature is minimized.

Since all calculations are run under steady-state conditions, it means that the whole heat produced by the volume is evacuated through the small heat sink. It is worth noting that the material generating heat (Ω_0) and high conductivity material (Ω_1) are viewed as homogenous and isotropic, without temperature effect on their respective conductivity. The geometrical and physical parameters are displayed on Fig. 2 for an arbitrary distribution of Ω_1 and are set as follow:

- the thermal conductivities are constant, with $k_0 = 1\, W/(m^2.K)$ and $k_1 = 100\, W/(m^2.K)$;
- the heat generation rates are assumed to be equal and constant with $q_0 = q_1 = 10\, kW/m^2$;

- all structures have a square aspect ratio ($L = H = 0.1\ m$), with a heat sink located in the middle of their left-hand side;
- with the exception of the heat sink which is characterized by a Dirichlet boundary condition ($T_d = 0\,°C$), all the other boundaries are adiabatic ($\nabla T \cdot n = 0$).

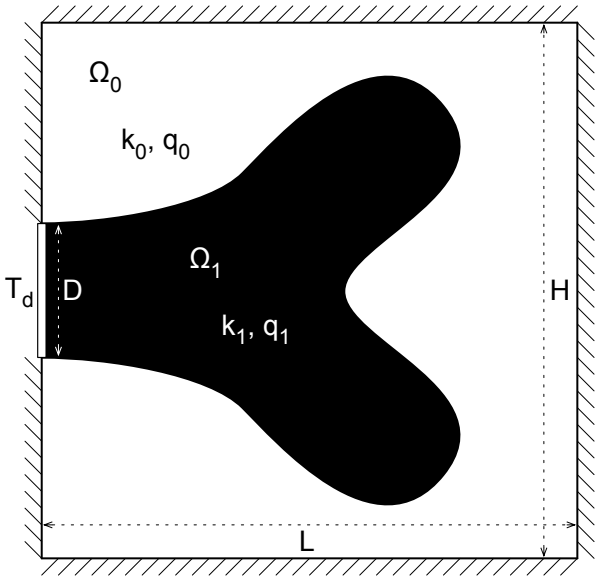

Figure 2: Academic study case aiming at cooling down a finite-size volume generating heat, closed by adiabatic boundary conditions with the exception of a small heat sink. This one is characterized by a Dirichlet boundary condition, at temperature T_d, located in the middle of the left-hand side boundary condition with a length D.

The results of the bi-objective optimization problem, as well as the influence of the volume constraint, are pictured on Fig. 3. For each volume constraint, $\overline{\varphi} = 0.1$ and $\overline{\varphi} = 0.125$, multi-objective optimizations have been run by discretizing $w \in [0, 1]$ with 101 elements, after rescaling each objective function according to Eq. (6). Fig. 3 displays a few results, sorted by volume constraint and weighting:

- Each column displays the structures reached from the two different volume constraints with a constant weighting w. Concretely, adding more high-conductivity material k_1 leads to strengthen the main V-shape, while adding new smaller scales to the existing high conductivity paths.
- Each row shows the evolution of solutions for $w = 0$, 0.5 and 1, *i.e.* from minimizing the temperature variance to minimizing the mean temperature over Ω. The main point is structural: the discontinuities existing for the structures reached from the temperature variance minimization are quickly reattached to the main tree, as clearly underlined by Figs. 3b and 3e.

The main structural difference between mean and variance temperature minimization lies on the discontinuity of the variance configuration displayed on Figs. 3a and 3d, compared to the uninterrupted connection of k_1 elements in Figs. 3c and 3f. Fig. 4 shows a deeper analysis of this specific feature from a physical point of view, by manually degrading the optimal solution

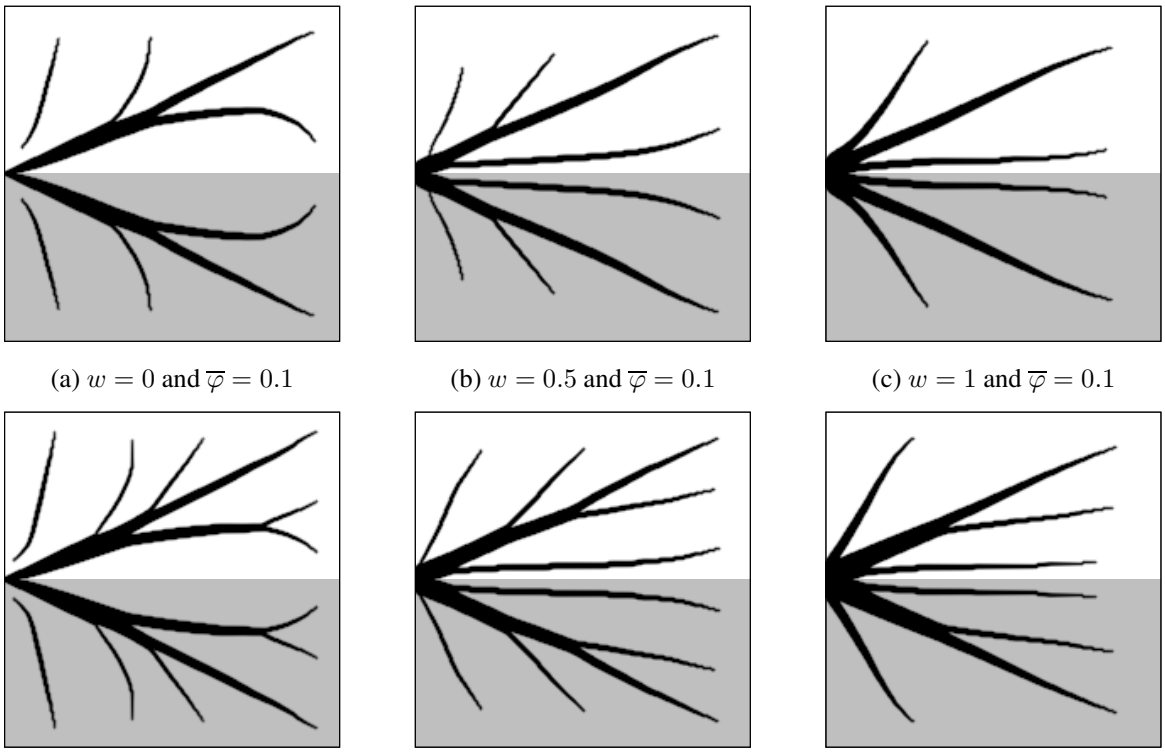

(a) $w = 0$ and $\overline{\varphi} = 0.1$ (b) $w = 0.5$ and $\overline{\varphi} = 0.1$ (c) $w = 1$ and $\overline{\varphi} = 0.1$

(d) $w = 0$ and $\overline{\varphi} = 0.125$ (e) $w = 0.5$ and $\overline{\varphi} = 0.125$ (f) $w = 1$ and $\overline{\varphi} = 0.125$

Figure 3: Numerical results for the topology optimization of two subdomains Ω_0 and Ω_1 made of different thermal conductivities k_0 and k_1 for the finite-size volume generating heat case. The solutions on each row correspond to two different volume constraints, respectively $\overline{\varphi} = 0.1$ and $\overline{\varphi} = 0.125$. The solutions on each column are computed with different weighting when linearly combining the functionals $J = w\hat{J}_1 + (1-w)\hat{J}_2$.

(Fig. 4a). In the absence of discontinuous structures, two vertical temperature gradients take place between the heat sink and the northern and southern areas 4b. Therefore, the two discontinuous high conductivity strips allow draining the heat flux towards the heat sink, without evacuating it. Indeed, if those were linked to the main Ω_1 structure, such as done in Fig. 4c, both temperature gradients would appear again because the cold area next to the heat sink would spread through the domain Ω_0. Consequently, it would not contribute to make homogeneous the temperature field.

The Pareto Fronts, reached from the 101 different weightings of $J_1(\eta)$ and $J_2(\eta)$ objective functions, are displayed in Fig. 5. Those are plotted for three different volume constraints, respectively $\overline{\varphi} = 0.1$ ($\circ$), $\overline{\varphi} = 0.125$ ($+$) and $\overline{\varphi} = 0.15$ ($\bullet$). From a thermal point of view, it underlines the impact of adding k_1 material, decreasing both objective functions $J_1(\eta)$ and $J_2(\eta)$ and shifting the Pareto frontiers towards its origin. This transformation takes place inside the white area in Fig. 5, since both limits of Pareto frontiers stand for the single objective minimization of $J_1(\eta)$ or $J_2(\eta)$: these two values decrease when enlarging the volume constraint, constricting the front within a smaller space.

Another point highlighted by Fig. 5 is the optimality of a few solutions, thanks to the convex shape of the Pareto frontiers. For each front, the weightings around $w = 0.5$ provide structures having both $J_1(\eta)$ and $J_2(\eta)$ minima close to their single objective minimization. This behaviour is obvious for $\overline{\varphi} = 0.15$ ($\bullet$), where $J_1 = 4.0\,^\circ C$ and $J_2 = 0.97\,^\circ C^2$, compared

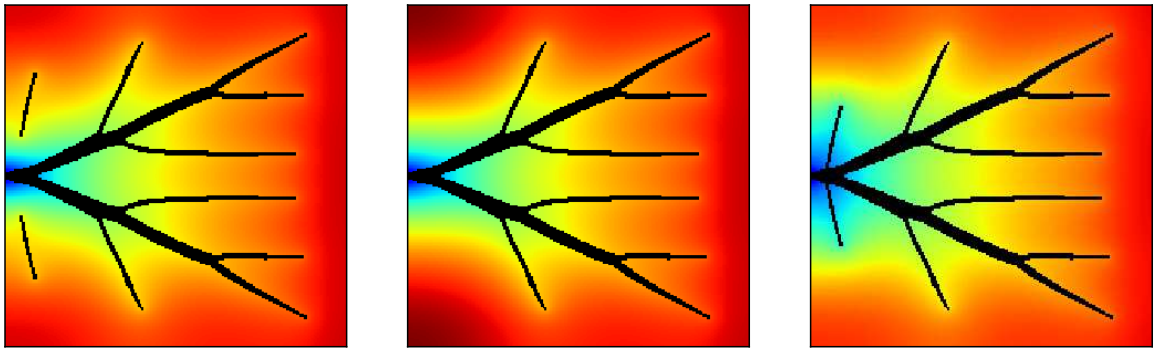

(a) Optimized solution ($J_2 = 2,33\,°C^2$).

(b) Optimized solution with manually deleted branches ($J_2 = 2,68\,°C^2$).

(c) Optimized solution with manually connected branches($J_2 = 2,76\,°C^2$).

Figure 4: Optimality analysis of non-connected patterns reached in structures minimizing the functional J_2.

with their respective single objective value $\underline{J_1} = 3.9\,°C$ $\underline{J_2} = 0.74\,°C^2$. In other words, this configuration takes advantage of both optimal design features computed with $w = 0$ and $w = 1$.

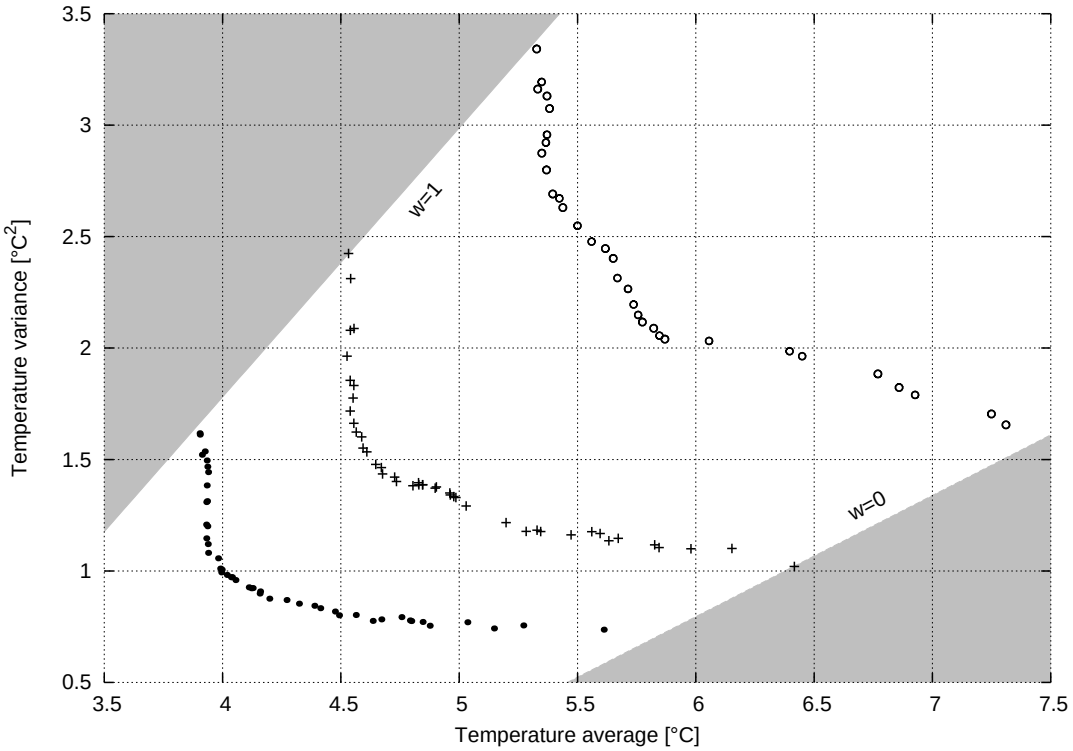

Figure 5: Pareto frontiers of J_1 (x-axis) and J_2 (y-axis) minimization problem established for 3 different volume constraints: $\overline{\varphi} = 10\%$ ($\circ$), $\overline{\varphi} = 12.5\%$ ($+$) and $\overline{\varphi} = 15\%$ ($\bullet$) for the finite-size volume generating heat case.

4 OPTIMAL SHAPE FOR CONVECTIVE HEAT TRANSFER

From now on, the domain Ω is made of a fluid and solid subdomains, respectively denoted Ω_f and Ω_s. Fluid is assumed to be Newtonian and incompressible, under laminar regime. It

is characterized by its dynamic viscosity μ, its thermal heat capacity C_p, its density ρ and its thermal conductivity k_f. Conversely, solid subdomain are only characterized with a thermal conductivity k_s. The approach chosen here locally adds an internal friction force between the fluid and a small obstacle in the same way as the Darcy's law within a porous media [11]. This new inverse permeability coefficient, denoted α, ranges from 0 to a sufficiently large value to create a momentum sink modelling the behaviour of solid subdomains. As previously explained, this additional term allows solving only one set of equations for both subdomains, if the α and k coefficients of Navier-Stokes and energy transport equations are properly fitted. Following the assumptions made in this section, the optimization problem writes

$$\begin{aligned} \inf_{\chi_{\Omega_f} \in \mathcal{D}_{\overline{\varphi}}} \quad & J(\mathbf{u}, P, T) \\ \text{subject to} \quad & \nabla \cdot \mathbf{u} = 0 \\ & \rho(\mathbf{u} \cdot \nabla)\mathbf{u} + \alpha(\chi_\omega)\mathbf{u} = -\nabla P + \mu \nabla^2 \mathbf{u} \\ & \rho C_p (\mathbf{u} \cdot \nabla) T = \nabla \cdot (k(\chi_\omega) \nabla T) \end{aligned} \tag{11}$$

where $\mathcal{D}_{\overline{\varphi}} = \{\chi_{\Omega_f} \in L^\infty(\Omega, \{0,1\}),\ |\Omega_f| \leq \overline{\varphi}|\Omega|\}$ and $\alpha(\chi_{\Omega_f})$ and $k(\chi_{\Omega_f})$ are domain dependent. The boundary conditions detailed in section 1 have to be added to the constraint definition as well. The functions α and k behaves in the following way: if $\mathbf{x} \in \Omega_f$, then $\alpha(1) = 0$ and $k(1) = k_f$. Conversely, if $\mathbf{x} \in \Omega_s$, then $\alpha(0) \to \infty$ and $k(0) = k_s$. Further details about the definition of α and k can be found in [19]. Also note that different parameters $\mathbf{p}$ are also used for penalizing these both parameters.

The Navier-Stokes and energy equations are discretized with the finite volume method, and computed with the so-called SIMPLER algorithm, which allows solving the pressure-velocity coupling [24]. Furthermore, an additional correction is included to properly take into account the viscous dissipation caused by the wall shear stress along the solid domain (see [19] for details).

4.1 Objective functions

The heat and mass transfer optimization problem introduced as so far is function of a generic objective function depending explicitly on $\mathbf{u}$, P and T, and implicitly on χ_{Ω_f}. This section aims at defining the physical goals pursue by the optimization process and gives them a mathematical formulation.

First, the objective function $J_1(\eta)$ is relative to minimizing the mechanic power dissipated by the fluid through the domain Ω and can be computed thanks to the total pressure losses as

$$J_1(\mathbf{u}, P) = -\int_\Gamma \left(P + \frac{1}{2}\rho|\mathbf{u}|^2 \right) (\mathbf{u} \cdot \boldsymbol{n})\, dx, \tag{12}$$

where Γ is the boundary of Ω domain. This objective is similar to minimizing the mechanical power spent to set the fluid into motion. Secondly, the objective function J_2 aims at maximizing the thermal power recovered from the domain Ω, by means of the inlet and outlet flow boundary conditions. This net thermal power is given by

$$J_2(\mathbf{u}, T) = \rho C_p \int_\Gamma T(\mathbf{u} \cdot \boldsymbol{n})\, dx \tag{13}$$

Therefore, the challenge is to conjointly optimize J_1 and J_2 in order to reach a configuration being a trade-off between both objectives: this means that further maximization of the thermal

power extracted by the fluid involves increasing the mechanical losses, and conversely. This problematic is really similar to the one encounters in the optimization of thermal heat exchangers, where manufacturers seek for the highest thermal transfer rates, while spending the lowest pumping power as possible.

For such bi-objective problem, the aggregated objective function $J(\eta)$ now writes

$$J(\mathbf{u}, P, T) = (1 - w)\hat{J}_1(\mathbf{u}, P) - w\hat{J}_2(\mathbf{u}, T). \tag{14}$$

Note that the thermal objective $\hat{J}_2$ is negatively weighted because it has to be maximized.

4.2 Numerical results

The study case is a square-shaped domain of side $\ell = 0.1\,m$, displayed in Fig. 6. The inlet and outlet flows are horizontally lined up in front of each other, with the same Poiseuille $\mathbf{u}-$velocity profiles. The inlet flow temperature is set to $T_i = 0\,°C$ and the vertical walls are assumed to be adiabatic. The horizontal walls closing the domain are subject to a constant temperature $T_w = 10\,°C$. The Reynolds number of this system, computed on the basis of the characteristic dimension $\ell/5$ and the average inlet velocity, is $Re = 3$. The thermal parameters are the following: $k_s = 10\,W/(m.K)$, $k_f = 1.0\,W/(m.K)$, and $C_p = 5.0\,kJ/(kg.K)$. The domain is discretized with 100×100 design elements and the volume constraint is $\overline{\varphi} = 0.4$.

Figure 7 displays the bi-objective optimization results that are reached by gradually increasing the weighting w. Four main classes of solution can be distinguished from their respective topology:

- For $w = 0$, the fluid is transported through a direct pipe, as expected from a physical point of view.
- For $0.06 \leq w \leq 0.12$, a solid core takes place at the center of the domain, splitting the fluid subdomain into a lower and an upper flows, as shown from Figures 7b to 7d. This moves both flows towards the lower and upper walls at constant temperature T_w, heating up the fluid without the temperature losses induced by the heat flux conduction through the solid domain. The more the w weighting increases, the more the central core width increases.
- For $0.26 \leq w \leq 0.60$, the central core is vertically split into several sub-cores, as shown from Figures 7e to 7g. This behavior breaks the horizontal temperature gradient through the solid core, by inserting one or more strips of fluid acting like a heat insulation material. Further details about this phenomenon are provided below.
- For $w = 0.75$, the surface of solid and fluid interfaces closed to the boundary conditions T_w are artificially increased by small solid inserts. This feature increases the main surfaces taking part into the heat transfer process.

Figure 8 displays the results for $w = 0$, minimizing the power lost by viscous dissipation within the fluid domain. As underlined by Figure 8a, the flow straightforwardly joins the inlet and outlet boundary conditions, with the largest fluid domain as possible. This aims at letting Ω_f being as wide as allowed by the constraint $\varphi(\eta) \leq \overline{\varphi}$ in order to minimize the shears inside the fluid flow. Figure 8b gives details about the pressure field within the Ω_f domain, which mainly follows an horizontal gradient. Figure 8c highlights both physical configurations for the heat transfer:

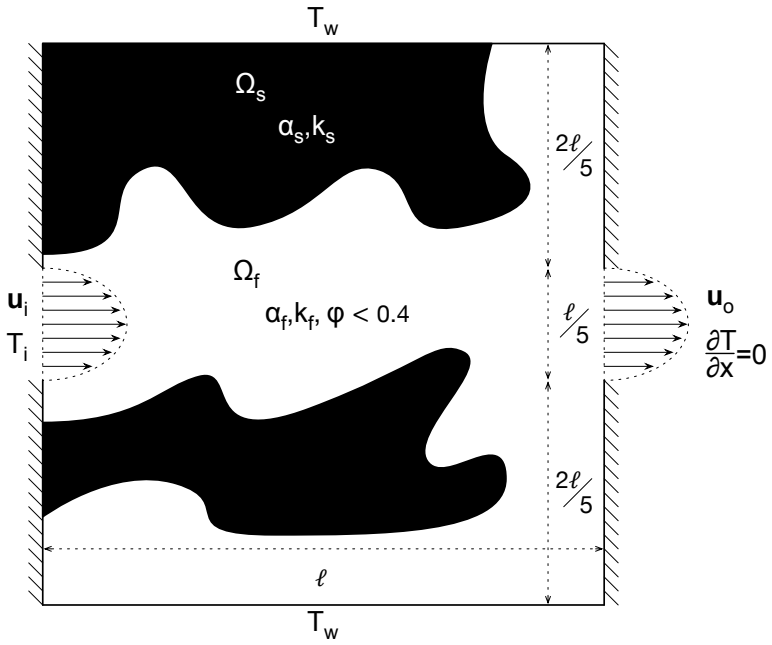

Figure 6: Academic study case aiming at maximizing the fluid outlet temperature, while minimizing the viscous dissipation through the fluid flow. Inlet and outlet flow boundary conditions face each other and are assumed to be driven by a Poiseuille flow. In addition, the vertical walls are adiabatic ($\nabla T \cdot n = 0$) and the upper and lower walls are set to a constant temperature T_w. Solid domain is pictured in black and indexed with s, whereas the fluid phase is pictured in white and indexed with f.

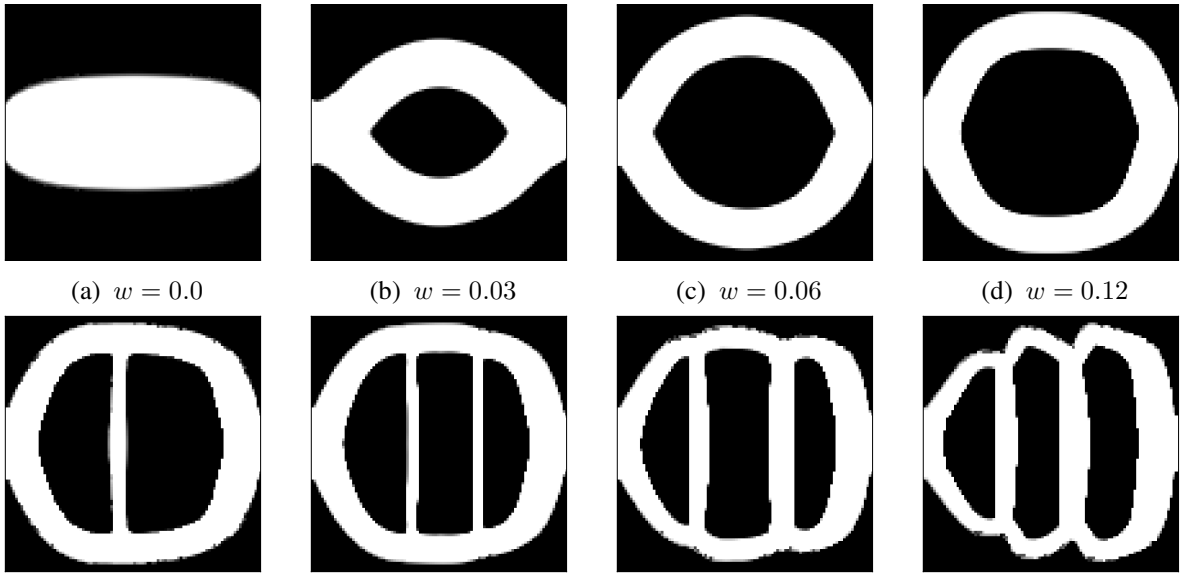

(a) $w = 0.0$ (b) $w = 0.03$ (c) $w = 0.06$ (d) $w = 0.12$

(e) $w = 0.26$ (f) $w = 0.28$ (g) $w = 0.60$ (h) $w = 0.75$

Figure 7: Optimal structures depending on w weighting.

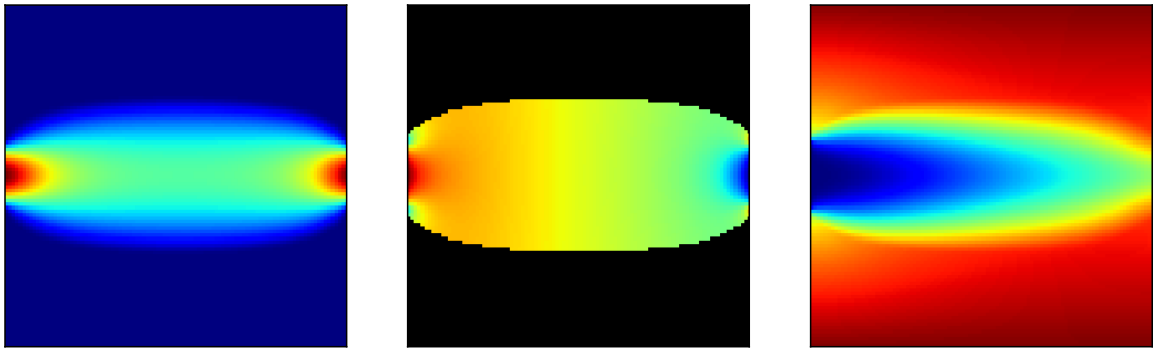

(a) $0 \leq |\mathbf{u}| \leq 1 \times 10^{-3}$ m/s (b) $-2.1 \leq P \leq 0 \times 10^{-3}$ Pa (c) $0 \leq T \leq 10\,^{\circ}$C

Figure 8: Minimization of the viscous dissipation in Ω for $w = 0$. The different state variables are pictured from left to right: velocity magnitude (a), pressure (b) and temperature (c).

- conduction within the solid domain, which mainly remains at temperatures close to T_w;
- conducto-convection within the fluid flow, which mainly transports the energy in its lower and upper boundary layers.

Figure 9 demonstrates the interest of splitting the central core in several different parts. Since $k_f < k_s$, the fluid areas having a zero-velocity field can be seen as an insulation material from the heat flux point of view. From a conductive point of view, the fluid strips act as large thermal resistances for the heat flowing through the solid core. The central field temperature is deeply affected by these discontinuities, as underlined by Figs. 9a and 9b. The temperature profile along the $x-$axis also shows the temperature gaps resulting from the "insulating fluid material" between each subcore, as plotted on Fig. 9e.

Without the strips of fluid, an horizontal temperature gradient would take place through the core, driving the heat flux from the near outlet flow area to the near inlet one (see Figs. 9c and 9d). Consequently, the outlet flow would be cooled by conduction through the central core, penalizing the objective function J_2. In other words, dividing the central part allows the temperature homogenization for each of its subset by restricting heat conduction, and ensures that both extreme parts are mainly under the influence of their closest thermal boundary condition.

One other interesting point underlined by Figure 9a is the presence of homogenized areas along the fluid/solid interfaces. Indeed, even if this solution seems to be fully converged, the solid boundaries remain rough: they are made of an artificial porous media. The split core may also be seen as a numerical manifestation of the homogenization process, since a core made of an infinite succession of vertical solid and fluid layers would perform better than any other one, for the same reasons as those aforementioned.

5 CONCLUSION

In this proceeding, we show that topology optimization may be successfully applied for the optimization of heat and mass transfers, mainly for the conductive and convective modes. It also underlines that multi-objective optimization is a reasonable method to tackle such problems and that interesting structural trade-offs between the different objectives could be reached. The numerical investigations reveal that most optimized structures are not trivial from a structural point of view, especially when they reached non-connected patterns.

The convective test case illustrates the main problematic of heat and mass transfers, consisting in increasing the thermal heat exchange with the fluid, while reducing as far as possible the

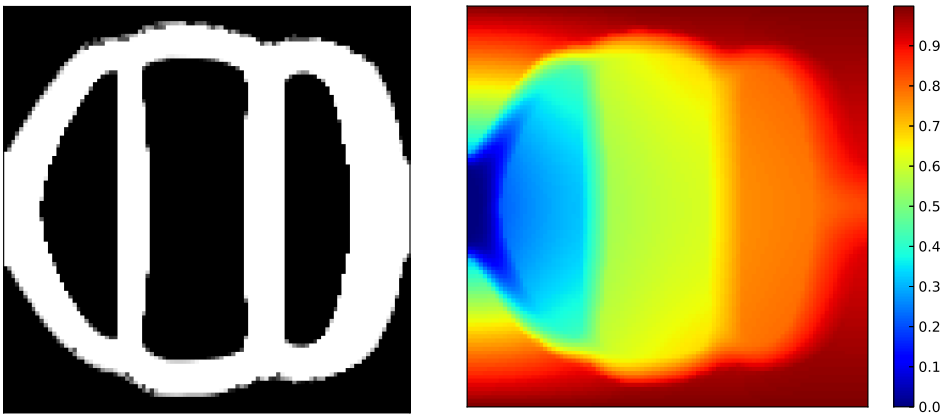

(a) η (b) $(T - T_i)/(T_w - T_i)$

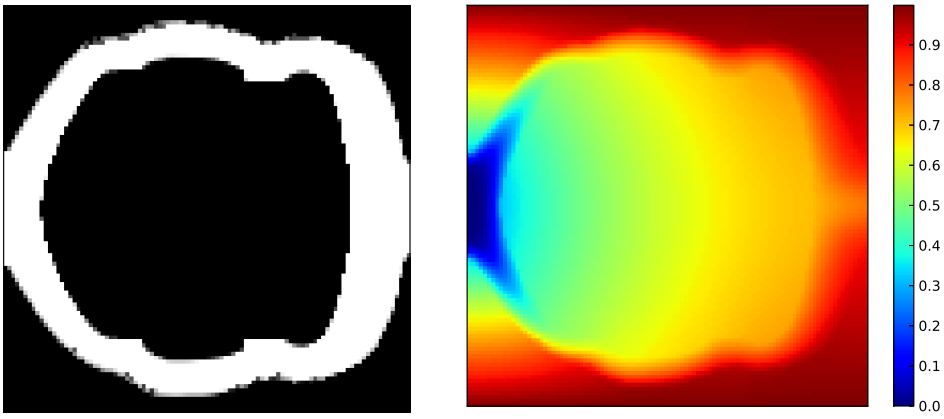

(c) η (d) $(T - T_i)/(T_w - T_i)$

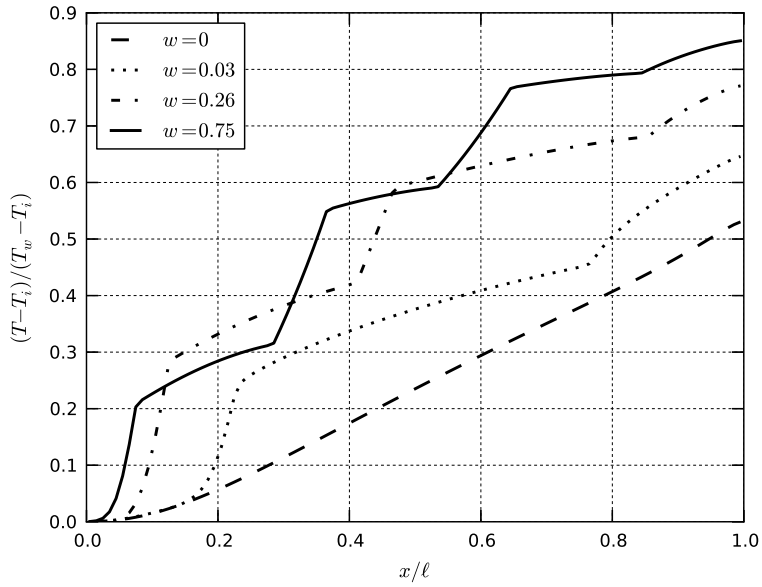

(e) Horizontal temperature profile for $y = 0.5\ell$.

Figure 9: Analysis of the core fragmentation from a thermal point of view.

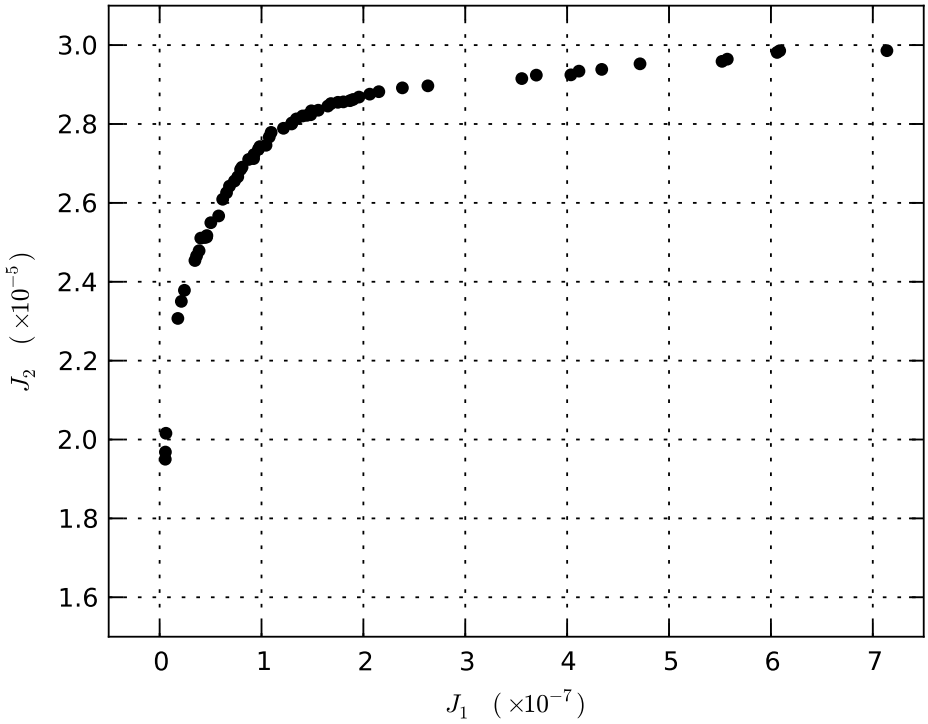

Figure 10: Pareto front corresponding to the minimization of J_1 (x-axis) and the maximization of J_2 (y-axis) established for the volume constraint $\overline{\varphi} = 0.4$.

power required to set it in motion. In this case, the aggregated objective function is proven to be a suitable approach, since the Pareto front of the problem is almost fully convex.

However, the topology optimization method, that transforms a shape optimization problem into a parametric one, raises several theoretical and numerical issues, such as the well-known homogenization phenomenon detailed in [1]. The numerical observation of this anomaly is made possible thanks to the problem relaxation, but should also be investigated from a theoretical point of view. It is worth nothing that the numerical experiments tend to show that the more the weighting of the thermal objective is larger, the more the homogenization process become prominent. Further works have to be done in order to propose adequate remedies for this problem.

REFERENCES

[1] G. Allaire. *Shape Optimization by the Homogenization Method*, volume 146 of *Applied Mathematical Sciences*. Springer, 2002.

[2] M. Bendsoe and O. Sigmund. *Topology Optimization: Theory, Methods and Applications*. Springer, 2nd edition, 2003.

[3] A. Bejan. Constructal-theory network of conducting paths for cooling a heat generating volume. *International Journal of Heat and Mass Transfer*, 40(4):799–811, 1997.

[4] G. Marck, J.-L. Harion, M. Nemer, S. Russeil, and D. Bougeard. A new perspective of constructal networks cooling a finite-size volume generating heat. *Energy Conversion and Management*, 52(2):1033–1046, 2011.

[5] R. Boichot, L. Luo, and Y. Fan. Tree-network structure generation for heat conduction by cellular automaton. *Energy Conversion and Management*, 50(2):376–386, 2009.

[6] L. Gosselin, M. Tye-Gingras, and F. Mathieu-Potvin. Review of utilization of genetic algorithms in heat transfer problems. *International Journal of Heat and Mass Transfer*, 52(9-10):2169–2188, 2009.

[7] C. Zhuang, Z. Xiong, and H. Ding. Topology optimization of multi-material for the heat conduction problem based on the level set method. *Engineering Optimization*, 42(9):811–831, September 2010.

[8] C. Zhuang, Z. Xiong, and H. Ding. Topology Optimization of the Transient Heat Conduction Problem on a Triangular Mesh. *Numerical Heat Transfer, Part B: Fundamentals*, 64(3):239–262, May 2013.

[9] A. Gersborg-Hansen, M. Bendsoe, and O. Sigmund. Topology optimization of heat conduction problems using the finite volume method. *Structural and multidisciplinary optimization*, 31(4):251–259, 2006.

[10] G. Marck, M. Nemer, J.-L. Harion, S. Russeil, and D. Bougeard. Topology optimization using the SIMP method for multiobjective conductive problems. *Numerical Heat Transfer, Part B: Fundamentals*, 61(6):439–470, June 2012.

[11] T. Borrvall and J. Petersson. Topology optimization of fluids in Stokes flow. *International Journal for Numerical Methods in Fluids*, 41(1):77–107, 2003.

[12] A. Gersborg-Hansen. *Topology optimization of flow problems*. PhD thesis, Technical University of Denmark, 2007.

[13] J. Guest and J. Prévost. Topology optimization of creeping fluid flows using a Darcy–Stokes finite element. *International Journal for Numerical Methods in Engineering*, 66:461–484, 2006.

[14] S. Kreissl, G. Pingen, and K. Maute. Topology optimization for unsteady flow. *International Journal for Numerical Methods in Engineering*, 2011.

[15] E. Dede. Multiphysics topology optimization of heat transfer and fluid flow systems. In *COMSOL Conference*, 2009.

[16] E. M. Papoutsis-Kiachagias, E. A. Kontoleontos, A. S. Zymaris, D. I. Papadimitriou, and K. C. Giannakoglou. Constrained topology optimization for laminar and turbulent flows, including heat transfer. In CIRA, editor, *EUROGEN, Evolutionary and Deterministic Methods for Design, Optimization and Control*, Capua, Italy, 2011.

[17] E. A. Kontoleontos, E. M. Papoutsis-Kiachagias, A. S. Zymaris, D. I. Papadimitriou, and K. C. Giannakoglou. Adjoint-based constrained topology optimization for viscous flows, including heat transfer. *Engineering Optimization*, pages 1–21, 2012.

[18] G. Marck. *Optimisation Topologique des Transferts de Chaleur et de Masse - Application aux Échangeurs de Chaleur*. PhD thesis, Mines ParisTech University, 2012.

[19] G. Marck, M. Nemer, and J.-L. Harion. Topology Optimization of Heat and Mass Transfer Problems: Laminar Flow. *Numerical Heat Transfer, Part B: Fundamentals*, 63(6):508–539, June 2013.

[20] A. Henrot and M. Pierre. *Variation et optimisation de formes: Une analyse géométrique*. Springer, 2005.

[21] G. Allaire. *Conception optimale de structures*. Mathématiques et Applications. Springer, 2006.

[22] K. Svanberg. The Method of Moving Asymptotes – A new method for structural optimization. *International Journal for Numerical Methods in Engineering*, 24:359–373, 1987.

[23] K. Svanberg. A class of globally convergent optimization methods based on conservative convex separable approximations. *SIAM Journal on Optimization*, 12(2):555–573, 2002.

[24] H. Versteeg and W. Malalasekera. *An introduction to computational fluid dynamics - The finite volume method*. Pearson Education Limited, Harlow, 2nd edition, 2007.